Electronic Supplementary Material (ESI) for Nanoscale.
This journal is © The Royal Society of Chemistry 2016

Electronic Supplementary Information

Highly Flexible Resistive Switching Memory Based on Amorphous-Nanocrystalline Hafnium Oxide Films

Jie Shang,[‡a,b,c] Wuhong Xue,[‡a,b,c] Zhenghui Ji,[‡b,c] Gang Liu,[*b,c] Xuhong Niu,[b,c] Xiaohui Yi,[b,c] Liang Pan,[b,c] Qingfeng Zhan,[b,c] Xiao-Hong Xu[*a] and Run-Wei Li*

[a]Key Laboratory of Magnetic Molecules and Magnetic Information Materials of Ministry of Education, School of Chemistry and Materials Science, Shanxi Normal University, Linfen, Shanxi 041004, China

[b]CAS Key Laboratory of Magnetic Materials and Devices, Ningbo Institute of Materials Technology and Engineering, Chinese Academy of Sciences, Ningbo, Zhejiang 315201, China

[c]Zhejiang Province Key Laboratory of Magnetic Materials and Application Technology, Ningbo Institute of Materials Technology and Engineering, Chinese Academy of Sciences, Ningbo, Zhejiang 315201, China

E-mail: xuxh@dns.sxnu.edu.cn (Prof. X.-H. Xu); liug@nimte.ac.cn (Prof. G. Liu); runweili@nimte.ac.cn (Prof. R.-W. Li)

[‡]These authors contributed equally to this work.

According to the Schuller formula,[1]

$$d=\lambda/2[\sin\vartheta_{n+1}-\sin\vartheta_n] \quad (1)$$

where d is the film thickness, λ is the wavelength of the X-ray beam, ϑ_{n+1} and ϑ_n are the reflective angle of the neighboring maximum of the reflected X-ray beam, the thickness of the HfO_x layer is derived to be about 10 nm from the X-ray reflectivity (XRR) curve.

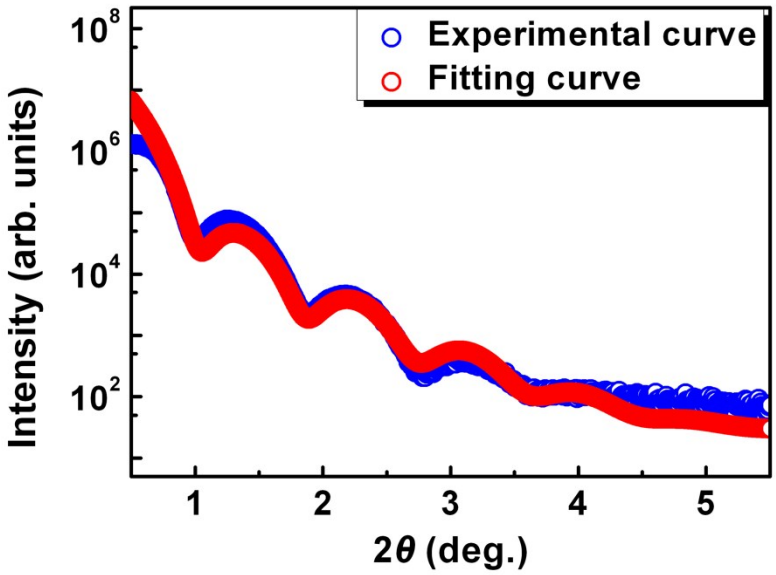

Fig. S1 X-ray reflectivity (XRR) and fitting curves of the as-deposited HfO_x.

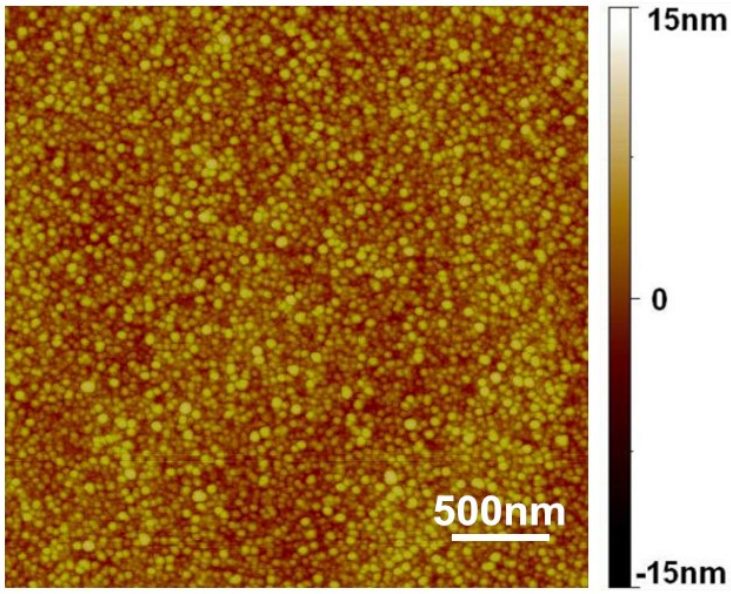

Fig. S2 Morphology of the HfO_x film grown on ITO/PET substrate.

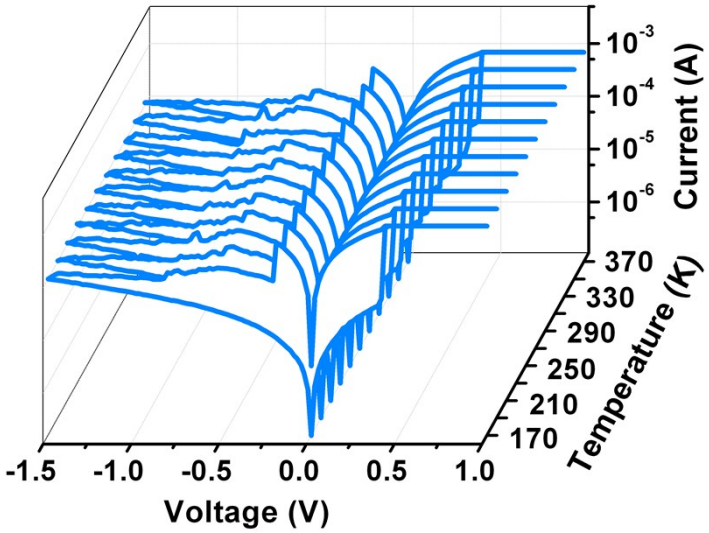

Fig. S3 I-V characteristics of the flat ITO/HfO_x/ITO/PET device in the temperature range of 170 K to 370 K.

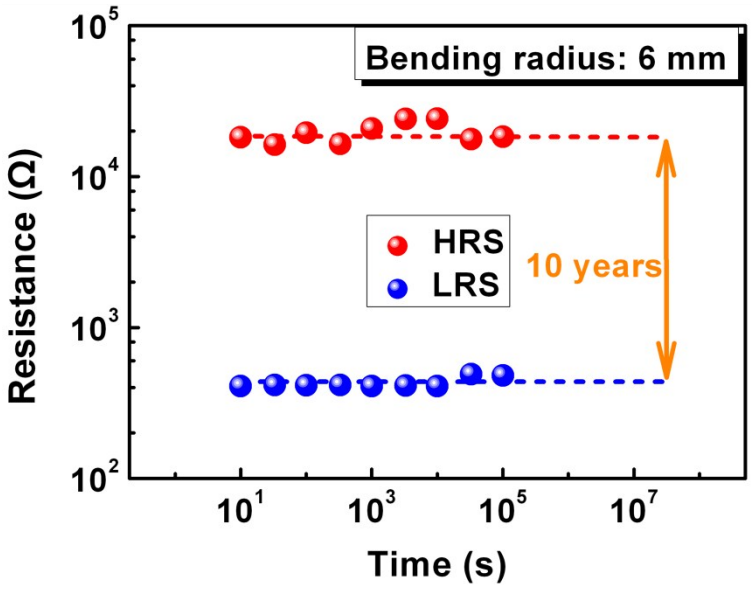

Fig. S4 Room temperature retention characteristics of the ITO/HfO_x/ITO/PET device at the bending radius of 6 mm or strain level of 1.06%. The device resistances at both HRS and LRS are read at 0.1 V.

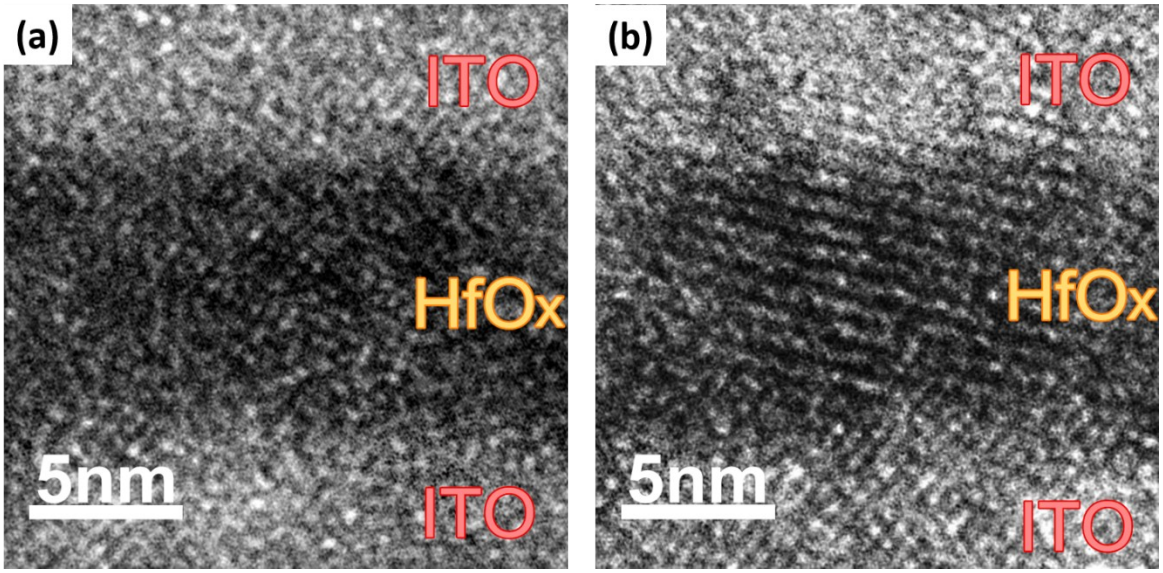

Fig. S5 Cross-sectional transmission electron microscopic image of the ITO/HfO_x/ITO device with (a) amorphous and (b) polycrystalline HfO_x microstructure.

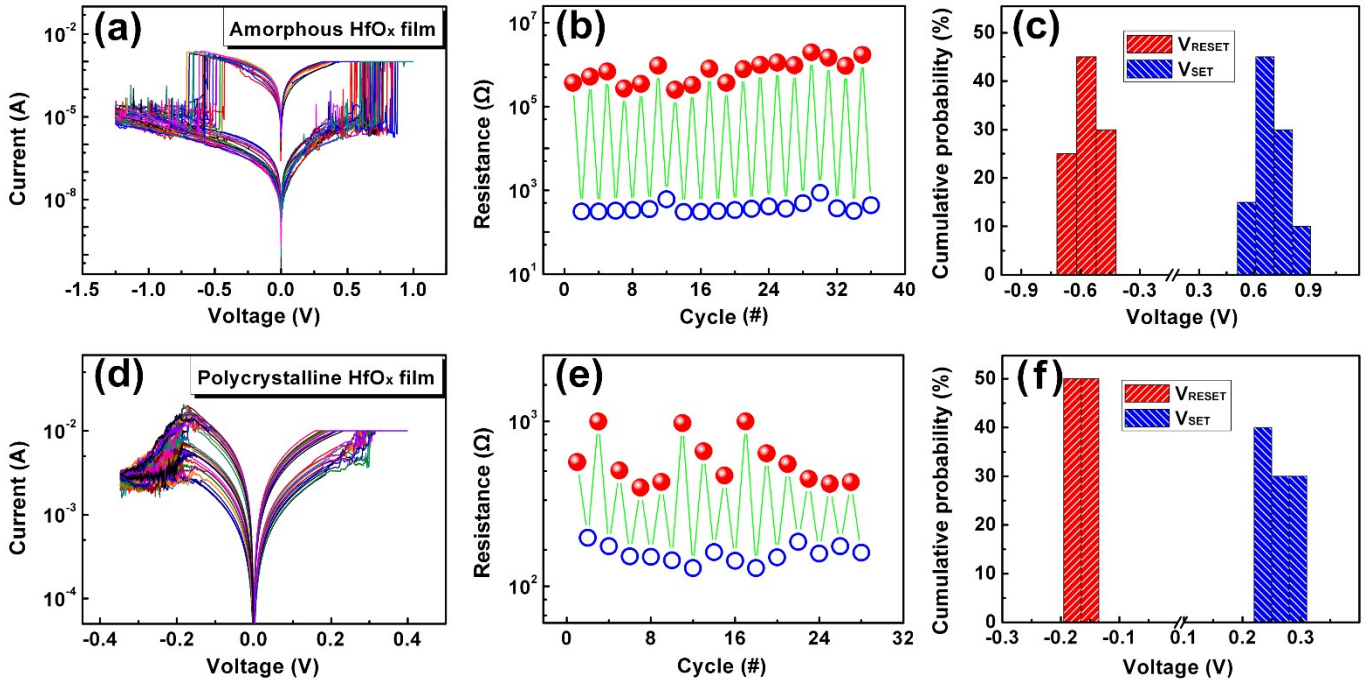

Fig. S6 (a) Current-voltage (I-V) characteristics of the ITO/amorphous HfO_x/ITO/PET structure in the flat state over 30 consecutive cycles at room temperature. (b) Room-temperature endurance characteristics of the switching device read at 0.01 V for both the high and low resistance states for the ITO/amorphous HfO_x/ITO structure. (c) Statistical distribution/cumulative probability of the set and rest voltages for the ITO/amorphous HfO_x/ITO structure. (d) I-V characteristics of the ITO/polycrystalline HfO_x/ITO/PET structure in the flat state over 20 consecutive cycles at room temperature. (e) Room-temperature endurance characteristics of the switching device read at 0.01 V for both the high and low resistance states for the ITO/ polycrystalline HfO_x/ITO structure. (f) Statistical distribution/cumulative probability of the set and rest voltages for the ITO/polycrystalline HfO_x/ITO structure.

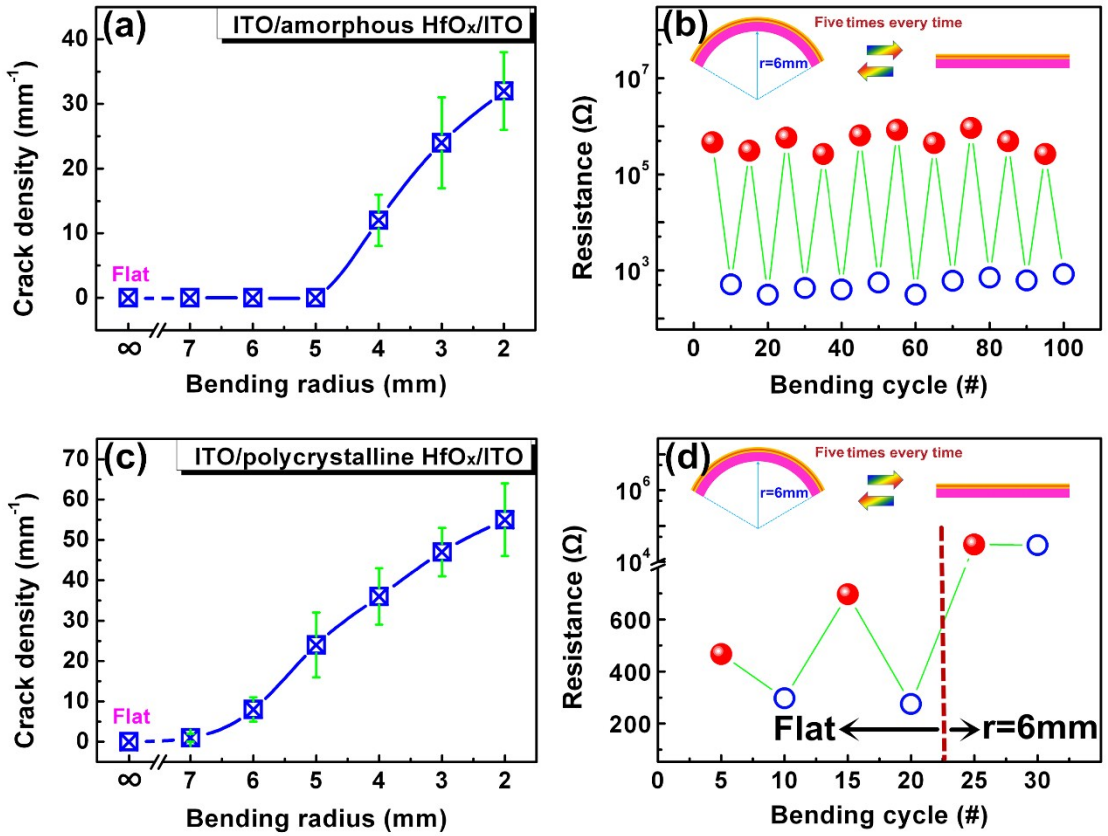

Fig. S7. (a) Plot of crack density vs. bending radius for the ITO/amorphous HfO_x/ITO/PET device. (b) Continuous bending fatigue test of the ITO/amorphous HfO_x/ITO/PET device with a radius of 6 mm for 100 cycles. (c) Plot of crack density vs. bending radius for the ITO/polycrystalline HfO_x/ITO/PET device. (d) Continuous bending fatigue test of the ITO/polycrystalline HfO_x/ITO/PET device with a radius of 6 mm for only 1 cycle.

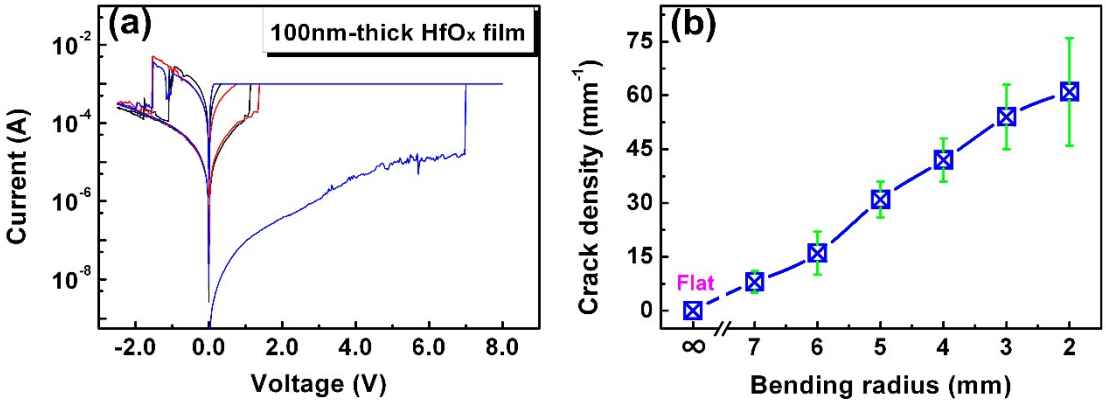

Fig. S8 (a) Current-voltage (I-V) characteristics of the ITO/100nm-thick nanocrystalline- amorphous mixed HfO_x/ITO/PET structure in the flat state at room temperature. (b) Plot of crack density vs. bending radius for the device.

Control experiments are also conducted to further clarify the microstructure-memory properties relationship of the hafnium oxide based devices. As shown in Fig. S5, both the amorphous and polycrystalline HfO_x thin films are obtained using different film deposition conditions. The switching behavior of the amorphous sample is similar to that of the nanocrystalline-amorphous device, except for the less uniformly distributed switching voltages (Fig. S6a-S6c). On the other hand, due to the presence of randomly distributed grain boundaries in the polycrystalline sample, branched conductive filaments would be formed in the switching layer. Serious leaking in the OFF state, as well as the severe fluctuation of the programming voltage and the device resistance are thus observed arising from the stochastic rupture and regeneration of the branched CFs (Fig. S6d-S6f). The mechanical performance of the ITO/amorphous HfO_x/ITO device is also similar to that of the nanocrystalline-amorphous device (Fig. S7a and S7b). The memory performance can be well maintained at the bending radius of 6 mm for ~ 100 consecutive bending cycles. As the bending radius drops less than 5 mm, cracks start to appear and the electrical varies accordingly. However, cracks appear much earlier in the polycrystalline control sample at the bending radius of 7 mm, and the device fails after being bended for only 30 cycles at the bending radius of 6 mm (Fig. S7c and S7d). When a much thicker HfO_x film (e.g. 100 nm) is used as the switching layer, an obvious forming process with the forming voltage of ~ 7 V is required to initialize the bistable switching behavior of the ITO/100 nm-HfO_x/ITO device. Cracks also appear earlier at the bending radius of 7 mm. Therefore, control experiments demonstrate that the nanocrystalline-amorphous mixed microstructure of the HfO_x film plays an important role in obtaining good mechanical flexibility and uniformity in resistive switching devices.

Table S1. Summary of switching performance of transparent RRAM devices

Device Structure	UV-Vis Transparency	$d(R_{OFF})$	$d(R_{ON})$	$d(V_{SET})$	$d(V_{RESET})$	References
AZO/Mg (30%)-doped ZnO/AZO/quartz glass	64% - 82%	24%	14.8%	12%	8.6%	2
ITO/Gd_2O_3/ITO/glass	>80%	61.9%	60%	50%	43.8%	3
AZO/ZnO/ITO/glass	55%-90%	~100%	/	/	/	4
IGZO/Ga_2O_3/IGZO/glass	~91.7%	73.9%	66.7%	/	/	5
Graphene/Dy_2O_3/ITO/glass	~80%	20%	100%	41.5%	27.3%	6
ITO/CeO_2/ITO/glass	81-73%	20%	15%	7%	/	7
ITO/ACG/ITO/glass	70-83%	57.8%	3.3%	15.1%	6.8%	8
Ga doped ZnO(GZO)/ZnO/ GZO/Sapphire	~80%	50%	25%	30%	20%	9
Ag/TiO_2/ITO/PET	~80%	60%	10%	/	/	10
ITO/HfO_x/ITO	~80%	12.8%	0.9%	7.9%	5.1%	This work

$d(R_{OFF})$, $d(R_{ON})$, $d(V_{SET})$, $d(V_{RESET})$ represent the dispersity coefficients of the OFF state resistance, ON state resistance, SET voltage and RESET voltage, respectively.

Table S2. Summary of switching performance of flexible RRAM devices

Switching Materials	Endurance	Retention	Bending Radius	Bending Endurance	Ref
GO	$>10^2$	$>10^5$ s	~8.0 mm	$>10^3$	11
Lu_2O_3	$>10^3$	$>10^5$ s	<5.0 mm	$>10^4$	12
NiO_X	$>10^2$	$>2.0\times10^4$ s	~5.0 mm	$>10^3$	13
SiO_x	>600	$>10^4$ s	<5.0 mm	>150	14
SnO_2	/	/	<7.0 mm	$>10^3$	15
TiO_2	$>10^2$	$>10^4$ s	<8.4 mm	$>10^3$	16
	$>10^2$	$>3.0\times10^4$ s	<10.0 mm	$>10^3$	17
WO_3	$>5.0\times10^3$	$>10^5$ s	<8.0 mm	$>2.0\times10^3$	18
Ag_2Se	$>10^4$	$>10^5$ s	<16 mm	$>10^2$	19
pEGDMA	>500	$>10^6$ s	<4 mm	$>10^3$	20
HKUST-1	>300	$>10^4$ s	<3.2 mm	>160	21
GeO_x/HfON	$>10^5$	$>10^4$ s	<9.0 mm	$>10^5$	22
PS + BCNT	>100	$>10^5$ s	<7 mm	>500	23
HfO_x	$>10^8$	$>10^5$ s	<5.0 mm	>1200	This work

References

1 Y. K. Schuller. *Phys. Rev. B*, 1980, **24**, 1597-1600.
2 X. Cao, X. M. Li, X. D. Gao, X. J. Liu, C. Yang, R. Yang, P. Jin. *J. Phys. D: Appl. Phys.*, 2011, **44**, 255104.
3 K.-C. Liu, W.-H. Tzeng, K.-M. Chang, Y.-C. Chan, C.-C. Kuo. *Microelectron. Eng.*, 2011, **88**, 1586-1589.
4 K. Y. Kim, E. L. Shim, Y. J. Choi. *J. Nanosci. Nanotechnol.* 2016, **16**, 10303-10307.
5 X. B. Yan, H. Hao, Y. F. Chen, Y. C. Li, W. Banerjee. *Appl. Phys. Lett.* 2014, **105**, 093502.
6 H. B. Zhao, H. L. Tu, F. Wei, J. Du. *IEEE T. Electron. Dev.* 2014, **61**, 1388-1393.
7 M. Ismail, A.M.Rana, I. Talib, T. -L. Tsai, U. Chand, E. Ahmed, M. Y. Nadeem, A. Aziz, N. A. Shah, M. Hussain.*Solid State Commun.* 2015, **202**, 28-34.
8 Y.-C. Chang, Y. -H. Wang. *Appl. Phys. Lett.* 2015, **106**, 123302.
9 P. Misra, A. K. Das, L. M. Kukreja. *Phys. Status Solidi C* 2010, **7**, 1718-1720.
10 K. N. Pham, V. D. Hoang, C. V. Tran, B. T. Phan. *Adv. Nat. Sci.: Nanosci. Nanotechnol.* 2016, **7**, 015017.
11 H. Y. Jeong, J. Y. Kim, J. W. Kim, J. O. Hwang, J.-E. Kim, J. Y. Lee, T. H. Yoon, B. J. Cho, S. O. Kim, R. S. Ruoff, S.-Y. Choi. *Nano Lett.* 2010, **10**, 4381-4386.
12 S. Mondal, J.-L. Her, K. Koyama, T.-M. Pan. *Nanoscale Res. Lett.* 2014, **9**, 3
13 S. Kim, J. H. Son, S. H. Lee, B. K. You, K. Park, H. K. Lee, M. Byun, K. J. Lee. *Adv. Mater.* 2014, **26**, 7480-7487.
14 G. Wang. A.-R. O. Raji, J.-H. Lee, J. M. Tour. *ACS Nano* 2014, **8**, 1410-1418.
15 M. Lyu, Y. Liu, Y. Zhi, C. Xiao, B. Gu, X. Hua, S. Fan, Y. Lin, W. Bai, W. Tong, Y. Zou, B. Pan, B. Ye, Y. Xie. *J. Am. Chem. Soc.* 2015, **137**, 15043-15048.
16 S. Kim, H. Y. Jeong, S. K. Kim, S.-Y. Choi, K. J. Lee. *Nano Lett.* 2011, **11**, 5438-5442.
17 D.-H. Lien, Z.-K. Kao, T.-H. Huang, Y.-C. Liao, S.-C. Lee, J.-H. He. *ACS Nano* 2014, **8**, 7613-7619.
18 L. Liang, K. Li, C. Xiao, S. J. Fan, J. Liu, W. S. Zhang, W. H. Xu, W. Tong, J. Y. Liao, Y. Y. Zhou, B. J. Ye, Y. Xie. *J. Am. Chem. Soc.* 2015, **137**, 3102-3108.
19 J. Jang, F. Pan, K. Braam, V. Subramanian. Adv. Mater. 2012, 24, 3573-3576.
20 B.-H. Lee, H. Bae, H. Seong, D. Lee, H. Park, Y. J. Choi, S.-G. Im, S. O. Kim, Y.-K. Choi. *ACS Nano* 2015, **9**, 7306-7313.
21 L. Pan, Z. H. Ji, X. H. Yi , X. J. Zhu, X. X. Chen, J. Shang, G. Liu, R.-W. Li. *Adv. Funct. Mater.* 2015, **25**, 2677-2685.
22 C.-H. Cheng, F.-S. Yeh, A. Chin. *Adv. Mater.* 2011, **23**, 902-905.
23 S. K. Hwang, J. M. Lee, S. Kim, J. S. Park, H. I. Park, C. W. Ahn, K. J. Lee, T. Lee, S. O. Kim. *Nano Lett.* 2012, **12**, 2217-2221.